Published in Physics Letters A 426 (2022) 127897

$Magnetoelectric\ effect\ in\ Ni_{1\text{--}x}Zn_xFe_2O_4/PZT\ thin\ film$

heterostructures

Peng Zhou^{1, 3}, Zhiqiang Zheng¹, Yajun Qi^{1, 3}*, Gopalan Srinivasan², Tianjin Zhang¹*

¹Ministry of Education Key Laboratory for Green Preparation and Application of Functional Materials, Hubei Provincial Key Laboratory of Polymers, Collaborative Innovation Center for Advanced Organic Chemical Materials Co-constructed by the Province and Ministry, Hubei University, School of Materials Science and Engineering, Hubei University, Wuhan 430062, PR China

²Physics Department, Oakland University, Rochester, Michigan 48309, USA

³Hubei Key Laboratory of Ferro & Piezoelectric Materials and Devices, Faculty of Physics & Electronic Science, Hubei University, Wuhan, 430062, China

Abstract: Magnetoelectric coupling effect of Ni_{1-x}Zn_xFe₂O₄/PZT (NZFO/PZT) thin film heterostructures is investigated by tuning the Zn content in NZFO film. The highest magnetoelectric coupling coefficient of NZFO/PZT heterostructures is achieved at x = 0.15 with the value of 328 mV/cm Oe. This various magnetoelectric effect in NZFO/PZT heterostructures with different Zn content is induced by distinct magnetostriction of NZFO film, which is related to piezomagnetic coefficient q of PZT layer, the initial permeability μ_i of NZFO layer, as well as the exchange interaction of ions at tetrahedral and octahedral sites. This study is of significance for understanding the magnetoelectric effects of epitaxial magnetoelectric heterostructures that involves NZFO ferrite films.

Key words: ferrite; magnetostriction; magnetoelectric effect

E-mail: yjqi@hubu.edu.cn (Y. J. Qi) zhangtj@hubu.edu.cn (T. J. Zhang)

Introduction

Magnetoelectric (ME) effect is defined as the dielectric polarization of a material in an applied

magnetic field or as an induced magnetization in an external electric field [1, 2]. Tuning of ME

effect of thin film heterostructures is an important research field in terms of the potential

applications in sensors, microwave devices, heterogeneous read/write devices and so on.

ME effect of multiferroic heterostructures is strongly dependent on the magnetostriction of

magnetic phase because of the intimate correlation between magnetic and ferroelectric phase. It

has been reported that magnetostriction as well as magnetization of Ni-Zn ferrite is determined by

Zn content [3-6]. Variation of Zn concentration usually leads to cation redistribution as Zn has a

strong preference for tetrahedral site (A-site) while Ni mostly occupies the octahedral site (B-site)

[7, 8]. ME interactions in Ni_{1-x}Zn_xFe₂O₄ and PZT composites have been investigated and the

maximum ME coupling coefficient is achieved with x of 0.2 [9]. For single phase multiferroics, 0.9

BaTiO₃-0.1 Ni_{1-x}Zn_xFe₂O₄ obtains the highest ME response as x of 0.2 [10]. So far, most of the

studies related to Ni-Zn ferrites have been focused on their magnetic/electrical properties and/or

bulk ME composites [11-17]. Systematic investigations on Zn content dependence of ME effect in

epitaxial thin film heterostructures of Ni-Zn ferrite and piezoelectric are still lacking. Hence,

studies on ME effect incorporating Ni-Zn ferrite and piezoelectric thin films will be helpful for

understanding the influence of Zn doped nickel ferrite on ME interaction.

In this work, Ni_{1-x}Zn_xFe₂O₄/Pb(Zr_{0.52}Ti_{0.48})O₃ (NZFO/PZT) epitaxial thin film heterostructures are

grown on (001) SrTiO₃ (STO) single crystalline substrates to investigate the relationship between

the amount of Zn doping and ME interaction, where x = 0, 0.1, 0.15, 0.2, and 0.25, respectively.

The highest ME coupling coefficient of 328 mV/cm Oe is achieved at x = 0.15. This phenomenon

of Zn content dependence of ME interaction in NZFO/PZT heterostructures is related to the magnetostriction of NZFO films.

Materials and methods

NZFO/PZT heterostructures with Zn content of 0, 0.1, 0.15, 0.2, and 0.25, were grown on SrRuO₃ (SRO) buffered (001) STO substrates via pulsed laser deposition. Appropriate stoichiometric single phase NZFO targets with different Zn substitution were used for the deposition. The NZFO targets were fabricated by conventional solid phase sintering. For detailed information on fabrication process please refer to our previous work ^[18]. Here, SRO is acted as bottom electrode while Pt (~ 73 nm) was deposited on NZFO as top electrode for electrical and ME measurements. To realize optimal ME response, thicknesses of NZFO and PZT films are fixed to ~ 160 nm and ~170 nm, respectively^[18]. The sample dimension is lenght×width×thickness = 3 mm× 3 mm× 160 nm. These heterostructures are labeled S-1, S-2, S-3, S-4, and S-5 for Zn content of 0, 0.1, 0.15, 0.2, and 0.25, respectively.

Structural properties of these heterostructures were characterized by X-ray diffraction (XRD) using Bruker D8 Discover four-circle diffraction system (Cu $K_{\alpha 1}$, $\lambda = 1.5406$ Å). Ferroelectric hysteresis loops were measured by a standard ferroelectric test system (Radiant Premier II, Radiant Technologies Inc.) at room temperature. Magnetization vs magnetic field loops (M-H) were measured by Physical Property Measurement System (PPMS, Quantum Design). ME coupling coefficient were characterized on a probe station with superconducting magnet (Lakeshore Model 625): ME voltage induced by an oscillating magnetic field was collected under different DC magnetic field via lock-in amplifier [19]. Cation distribution in NZFO films was analyzed via X-ray photoelectron spectroscopy (XPS, Thermo Fisher Scientific 250Xi).

Results and discussion

Figure 1(a) shows representative XRD θ -2 θ scan of sample S-4. Diffraction peaks from NZFO and PZT are discernable though the intensity for NZFO is relative weak. No other diffraction peak is observed except for the peaks from NZFO, PZT, SRO, and STO, indicating that all of the films are

grown along the direction normal to film plane. Representative ϕ -scan of sample S-1 is exhibited in figure 1(b), where the diffraction peaks occurs at regular interval of 90° for individual films and substrate. The position of diffraction peaks of individual films is in line with that of the substrate, demonstrating that all of the films are epitaxially grown on STO substrates. Epitaxial relationship between films and substrate can be written as: NZFO (004) [040] \parallel PZT (002) [020] \parallel SRO (002) [020] \parallel STO (002) [020]. Similar XRD results of other samples are not shown here. Symmetric and asymmetric XRD-Reciprocal Space Mappings (see Supplementary Information) reveal that all of the NZFO films are fully relaxed.

Ferroelectric hysteresis loop of PZT is shown in figure 2(a). The ratio of remanent polarization/saturation polarization as well as coercive electric field of PZT layer reaches 0.76 and 110 kV/cm, respectively, indicating that PZT layer has good ferroelectric property. The saturated magnetization (M_s) and coercive magnetic field (H_c) of NZFO layers can be obtained from magnetic hysteresis loops shown in figure 2(b), and their correlation with Zn content is illustrated in figure 2(c). On the one hand, M_s increases with the increase of Zn substitution except for the sample with Zn content of 0.2. This kind of trend, which is related to the distribution of magnetic ions (Ni²⁺ and Fe³⁺) and non-magnetic ions (Zn²⁺) in spinel network at tetrahedral and octahedral sites, is in line with what reported previously [5, 20, 21]. While the coercive magnetic field (Hc) decreases with the increase of Zn substitution, which can be understood on the basis of magnetocrystalline anisotropy. The anisotropy constant value of nickel ferrite is greater than that of Zn ferrite^[21]. Therefore, H_c for Zn substituted ferrite is lower. More substitution of Ni²⁺ by Zn²⁺ means lower Hc. On the other hand, M_s for nickel ferrite in current work is 104 emu/cm³, which is much smaller than its bulk value of 270 emu/cm³ [22]. In addition, M_s of 330 emu/cm³ for sample S-5 is lower than its bulk value of 375 emu/cm³ (assuming density of 5.368 g/cm³) [5]. The lower $M_{\rm s}$ in current work could be explained on pinning of moments due to presence of defects, such as antiphase boundaries, in the films [22].

ME response of NZFO/PZT heterostructures with various Zn content is exhibited in figure 3(a). The ME coupling coefficient is determined by $\alpha_{E31} = V_{out}/(d^*H_{ac})$, where V_{out} , d, and H_{ac} denote ME voltage, thickness of PZT layer, and amplitude of AC magnetic field, respectively^[23]. α_{E31} ,

which is obtained at H_{ac} of 3 Oe with frequency of 1 kHz at room temperature, increases first and then decreases after reaching the peak values for all of the samples. Variation of α_{E31} and H_{dc} (DC magnetic field corresponding to peak values) with Zn content is shown in figure 3(b). With the increase of Zn concentration, H_{dc} decreases monotonically while α_{E31} reaches its maximum value of 328 mV/cm Oe when Zn content is 0.15.

One possible cause for the observed highest α_{E31} at Zn content of 0.15 could be the noncollinear spin structure and the enhanced magnetostriction reported in previous studies on nickel zinc ferrite [4, 24]. These studies, however, were on Zn substitutions of 0.25 or more and at low temperatures. Satya Murthy et al. carried out neutron diffraction studies on nickel zinc ferrite with Zn substitutions varying from 0 to 1 [24]. The ordering was found to be Neel type in pure nickel ferrite and canting was observed upon Zn substitution for Ni and the canting angle θ decreased with increasing temperature. For Zn substitution of 0.25, θ decreased from 17.6 deg at low temperature to 10 deg at 100 K. At room temperature the ordering was collinear Neel type. Thus in our case canting related increase in the magnetostriction cannot be the cause of enhancement in the strength of ME coupling.

The key ingredients for the magnetic phase for achieving a large ME coupling strength in the composites are (i) the piezomagnetic coefficient q and (ii) the initial permeability μ_i . We attribute the observations in our case to enhancements in both parameters in Zn substituted nickel ferrites. Under an applied AC magnetic field, the field confinement in the composite critically depends on μ_i and the ME coefficient is directly proportional to q. Figure 3 (c) shows the variation in the ME coefficient for composites of polycrystalline platelets of NZFO and PZT and the dependence of the product $(q\mu_i)$ on Zn substitution (data from early report [25]). The product $(q\mu_i)$ increases with Zn substitution and shows a maximum for x = 0.4 whereas ME coefficient shows a maximum for composites with x = 0.3. In our case for ferrite films on substrate one expects significant departure in values of magnetic parameters from bulk values due to substrate clamping and it is reasonable to attribute the observation of enhancement in the ME coefficient for $x \sim 0.15$ to enhancement in both q and $\Box \mu_i$. Although direct measurements of these parameters will validate the proposed cause, we lack the essential facilities for such measurements.

In addition, magnetostriction effect in NZFO was reported to originate from dipolar interaction

among magnetic ions, the single ion contribution of Fe³⁺ at A and B sites, and the single ion contribution of Ni²⁺ at B sites^[4]. The exchange interaction of A-B ions is the strongest while that of A-A and B-B ions is the weakest^[6]. A and B sites are surrounded with four and six nearest-neighbor of O²⁻, respectively. Thus the crystal field at A and B sites are quite different. To further study the exchange interaction in A and B sites, XPS is used to analyze the cation distribution in NZFO films, as shown in figure 4. Figure 4(a) shows Zn 2p_{3/2} and Zn 2p_{1/2} core-level XPS spectra of NZFO layers with different Zn content. Both peaks from Zn 2p_{3/2} (~ 1021.2 eV) and Zn 2p_{1/2} (~ 1044 eV) except for the sample without Zn doping correspond to typical tetrahedrally coordinated Zn²⁺ states^[26-28], indicating that Zn takes only tetrahedral site for all of the Zn substituted samples. The XPS spectra of Fe 2p_{3/2}, Ni 2p_{3/2}, and O1s shown in figure 4(b) are asymmetric and can be deconvoluted into different lines. The shake-up satellite peak at \sim 718 eV for Fe 2p_{3/2} signals that Fe is in 3+ oxidation state^[29], and the other shake-up satellite peak at ~ 861 eV for Ni $2p_{3/2}$ is considered as the representative nickel peak^[30]. Detailed cation distribution in octahedral (B site) and tetrahedral (A site) sites is quantitatively estimated by calculating the deconvoluted peak areal ratio^[29]. The principle peak of Fe 2p_{3/2} is deconvoluted into two peaks located at ~ 710 eV (B site) and ~ 713 eV (A site). Similarly, the deconvoluted principle peak of Ni $2p_{3/2}$ is located at ~ 854 eV (B site) and ~ 855 eV (A site). As shown in figure 4(c), Fe³⁺ has the lowest distribution in B site for NZFO film with Zn content of 0.15, while the distribution for Ni²⁺ in B site increases monotonically with the increase of Zn content. For the deconvoluted O1s spectra, the peak occurs at ~ 530 eV is recognized as a typical M-O bond (M refers to metal), while the peaks at 531 eV and 532 eV are attributed to some defects and physical/chemical absorption of H₂O on sample surface, respectively^[30].

As mentioned above, the exchange interaction of A-B ions is the strongest while that of A-A and B-B ions is the weakest^[6]. Therefore, it's expected that the closer to 50% for Fe³⁺ and Ni²⁺ in B site distribution the stronger exchange interaction and magnetostriction would be. We can see that Fe³⁺ with Zn content of 0.15 and Ni²⁺ with Zn content of 0.25, respectively, have the closest distribution to 50%. The strongest magnetostriction would be reached when Zn content is in between 0.15 and 0.25. Hence, the possible reasons for the observed ME response in our case include piezomagnetic coefficient q of PZT layer, the initial permeability μ_i of NZFO layer, as well as the exchange interaction of ions at tetrahedral and octahedral sites.

Conclusions

In conclusion, ME effect of NZFO/PZT epitaxial thin film heterostructures is investigated by varying the Zn content in NZFO. Individual NZFO and PZT films show good magnetic and ferroelectric properties, respectively. α_{E31} is dependent on Zn content and it obtains the highest value of 328 mV/cm at Zn content of 0.15. The result of Zn content determined α_{E31} is attributed to piezomagnetic coefficient q of PZT layer, the initial permeability μ_i of NZFO layer, as well as the exchange interaction of ions at tetrahedral and octahedral sites. This work has significance to the area of ferrite-based magnetoelectric sensors.

Acknowledgements

This work was supported by the National Natural Science Foundation of China (No. 11974104), the China Postdoctoral Science foundation (No. 2020M672315), the Program of Introducing Talents of Discipline to Universities ("111 Project", D18025) China, and the Program of Hubei Key Laboratory of Ferro- & Piezoelectric Materials and Devices (No. K202013). The research at Oakland University was supported by grants from the Air Force Office of Scientific Research (AFOSR) Award No. FA9550-20-1-0114 and the National Science Foundation (DMR-1808892, ECCS-1923732)

References

- [1] G. Srinivasan, Magnetoelectric Composites. Annual Review of Materials Research **40**(1): 153-178 (2010)
- [2] C.-W. Nan, M. I. Bichurin, S. Dong, et al., Multiferroic magnetoelectric composites: Historical perspective, status, and future directions. Journal of Applied Physics **103**(3): 031101 (2008)
- [3] S. R. Murthy and T. S. Rao, Magnetostriction of Ni-Zn and Co-Zn ferrites. physica status solidi (a) **90**(2): 631-635 (1985)
- [4] K. I. Arai and N. Tsuya, Magnetostriction measurements of Ni-Zn ferrite single crystals. Journal of Physics and Chemistry of Solids **36**(5): 463-465 (1975)
- [5] M. Atif, M. Nadeem, R. Gr?Ssinger, et al., Studies on the magnetic, magnetostrictive and electrical properties of sol–gel synthesized Zn doped nickel ferrite. Journal of Alloys & Compounds **509**(18): 0-5724 (2011)

- [6] R. Adhikari, A. Sarkar, M. V. Limaye, *et al.*, Variation and sign change of magnetostrictive strain as a function of Ni concentration in Ni-substituted ZnFe2O4 sintered nanoparticles. Journal of Applied Physics **111**(7): 073903 (2012)
- [7] S. Ramesh, B. Dhanalakshmi, B. C. Sekhar, et al., Effect of Mn/Co substitutions on the resistivity and dielectric properties of nickel–zinc ferrites. Ceramics International **42**(8): 9591-9598 (2016)
- [8] X. Huang, J. Zhang, M. Lai, et al., Preparation and microwave absorption mechanisms of the NiZn ferrite nanofibers. Journal of Alloys and Compounds **627**: 367-373 (2015)
- [9] G. Srinivasan, C. DeVreugd, C. Flattery, et al., Magnetoelectric interactions in hot-pressed nickel zinc ferrite and lead zirconante titanate composites. Applied Physics Letters **85**: 2550-2552 (2004)
- [10] S. K. Upadhyay and V. R. Reddy, Study of 0.9 BaTiO3-0.1 NixZn1-xFe2O4 magneto-electric composite ceramics. Journal of Applied Physics **113**(11): 114107 (2013)
- [11] S. Nag, A. Roychowdhury, D. Das, et al., Structural and magnetic properties of erbium (Er3+) doped nickel zinc ferrite prepared by sol-gel auto-combustion method. Journal of Magnetism and Magnetic Materials **466**: 172-179 (2018)
- [12] C. M. Leung, G. Sreenivasulu, X. Zhuang, et al., A Highly Efficient Self-Biased Nickel-Zinc Ferrite/Metglas/PZT Magnetoelectric Gyrator. physica status solidi (RRL) Rapid Research Letters **12**(5): 1800043 (2018)
- [13] C. M. Leung, G. Sreenivasulu, X. Zhuang, et al., Stability enhancement of yttrium substituted nickel zinc ferrite/PZT magnetoelectric gyrators under high power conditions. Applied Physics Letters **112**(24): 242901 (2018)
- [14] D. Y. Karpenkov, A. A. Bogomolov, A. V. Solnyshkin, *et al.*, Multilayered ceramic heterostructures of lead zirconate titanate and nickel-zinc ferrite for magnetoelectric sensor elements. Sensors and Actuators A: Physical **266**: 242-246 (2017)
- [15] P. Liu, Z. Yao, J. Zhou, *et al.*, Small magnetic Co-doped NiZn ferrite/graphene nanocomposites and their dual-region microwave absorption performance. Journal of Materials Chemistry C **4**(41): 9738-9749 (2016)
- [16] X. Wu, W. Wu, L. Qin, et al., Structure and magnetic properties evolution of nickel–zinc ferrite with lanthanum substitution. Journal of Magnetism and Magnetic Materials **379**: 232-238 (2015)
- [17] D. Roy, S. Sakshath, G. Singh, *et al.*, Investigation on two magnon scattering processes in pulsed laser deposited epitaxial nickel zinc ferrite thin film. Journal of Physics D: Applied Physics **48**(12): 125004 (2015)
- [18] Z. Zheng, P. Zhou, Y. Liu, et al., Strain effect on magnetoelectric coupling of epitaxial NFO/PZT heterostructure. Journal of Alloys and Compounds: 152871 (2019)
- [19] J. Wang, Z. Fu, R. Peng, et al., Low magnetic field response single-phase multiferroics under high temperature. Mater. Horiz. **2**(2): 232-236 (2015)
- [20] A. P. C. Caizer, M. Stefanescu, C. Muntean, et al., Studies and magnetic properties of Ni-Zn ferrite synthesized from the glyoxilates complex combination. Journal of Optoelectronics and Advanced Materials **3** (2001)
- [21] P. Priyadharsini, A. Pradeep, P. S. Rao, et al., Structural, spectroscopic and magnetic study of nanocrystalline Ni–Zn ferrites. Materials Chemistry and Physics **116**(1): 207-213 (2009)
- [22] A. V. Singh, B. Khodadadi, J. B. Mohammadi, *et al.*, Bulk Single Crystal-Like Structural and Magnetic Characteristics of Epitaxial Spinel Ferrite Thin Films with Elimination of Antiphase Boundaries. Adv Mater **29**(30) (2017)
- [23] C. Deng, Y. Zhang, J. Ma, et al., Magnetoelectric effect in multiferroic heteroepitaxial BaTiO3-

NiFe2O4 composite thin films. Acta Materialia 56(3): 405-412 (2008)

[24] N. S. S. Murthy, M. G. Natera, S. I. Youssef, et al., Yafet-Kittel Angles in Zinc-Nickel Ferrites. Physical Review **181**(2): 969-977 (1969)

[25] G. Srinivasan, E. T. Rasmussen and R. Hayes, Magnetoelectric effects in ferrite-lead zirconate titanate layered composites: The influence of zinc substitution in ferrites. Physical Review B **67**(1) (2003)

[26] S. Bera, A. A. M. Prince, S. Velmurugan, *et al.*, Formation of zinc ferrite by solid-state reaction and its characterization by XRD and XPS. Journal of Materials Science **36**(22): 5379-5384 (2001)

[27] V. Šepelák and K. D. Becker, Comparison of the cation inversion parameter of the nanoscale milled spinel ferrites with that of the quenched bulk materials. Materials Science and Engineering: A **375-377**: 861-864 (2004)

[28] A. Bajorek, B. Liszka, B. Szostak, *et al.*, Microstructure and magnetism of Ni0.5Zn0.5Fe2O4/MWCNTs nanocomposites. Journal of Magnetism and Magnetic Materials **503**: 166634 (2020)

[29] N. Liu, P. Du, P. Zhou, et al., Annealing temperature effects on the cation distribution in CoFe2O4 nanofibers. Applied Surface Science **532**: 147440 (2020)

[30] X. Gao, W. Wang, J. Bi, et al., Morphology-controllable preparation of NiFe2O4 as high performance electrode material for supercapacitor. Electrochimica Acta (2018)

Figure Captions

Figure 1 XRD θ -2 θ scan of sample S-4 (a), and XRD ϕ -scan of sample S-1 (b)

Figure 2 (a) Ferroelectric hysteresis loops of PZT layer, (b) magnetic hysteresis loops of NZFO layers with different Zn content, (c) Zn dependence of M_s and H_c obtained from (b)

Figure 3 (a) ME coupling coefficient α_{E31} vs H_{dc} for heterostructures with different Zn content, (b) maximum α_{E31} and the related H_{dc} obtained from (a), (c) Variation in the ME coefficient for composites of polycrystalline platelets of NZFO and PZT and the dependence of the product (q μ_i) on Zn substitution. Figure adapted from ref. [25]

Figure 4 (a) XPS spectra of Zn $2p_{3/2}$ and Zn $2p_{1/2}$ for NZFO films with different Zn content, (b) Fe $2p_{3/2}$, Ni $2p_{3/2}$, and O1s core-level XPS spectra for NZFO films with different Zn content. The vertical dashed lines indicate the reference binding energies for octahedral sites, tetrahedral sites, satellite peaks, M-O bond, O_I, and O_{II}, (c) dependence of distribution of Fe and Ni in octahedral sites on Zn content.

Figure 1

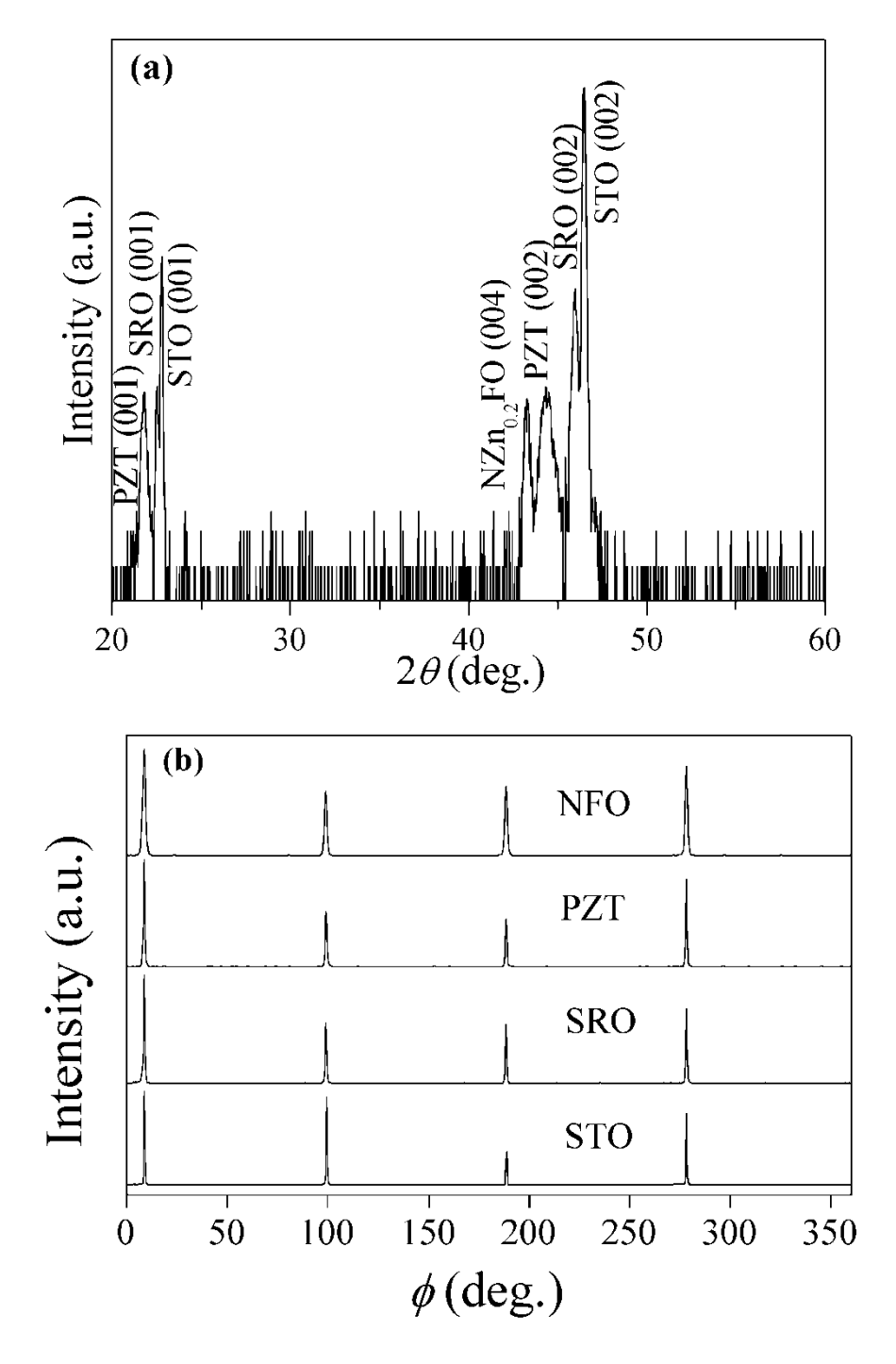
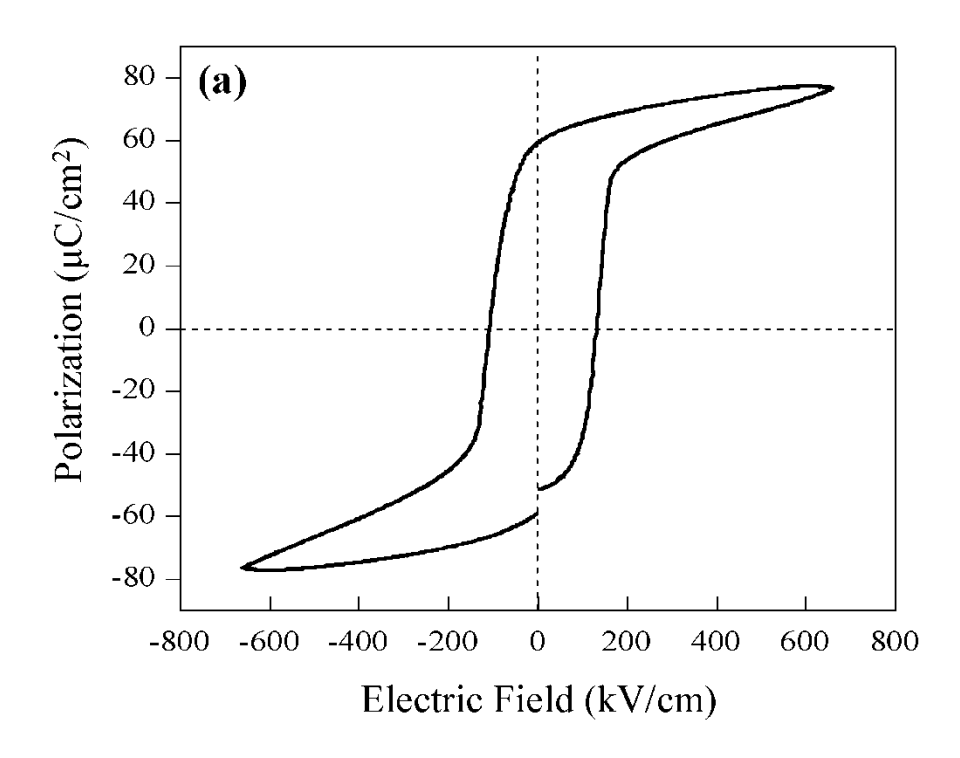
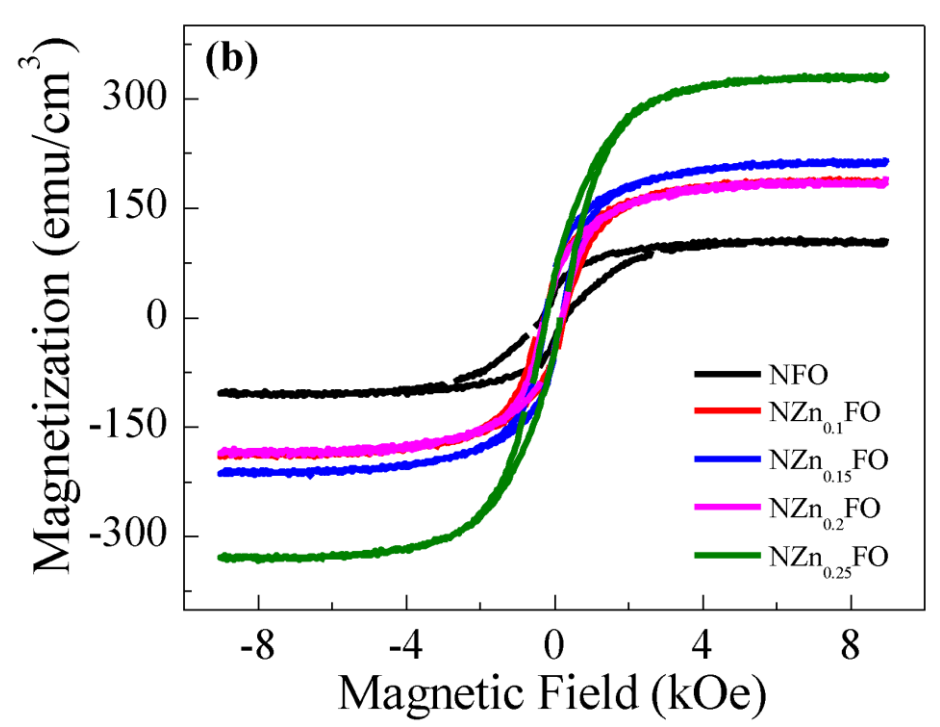


Figure 2





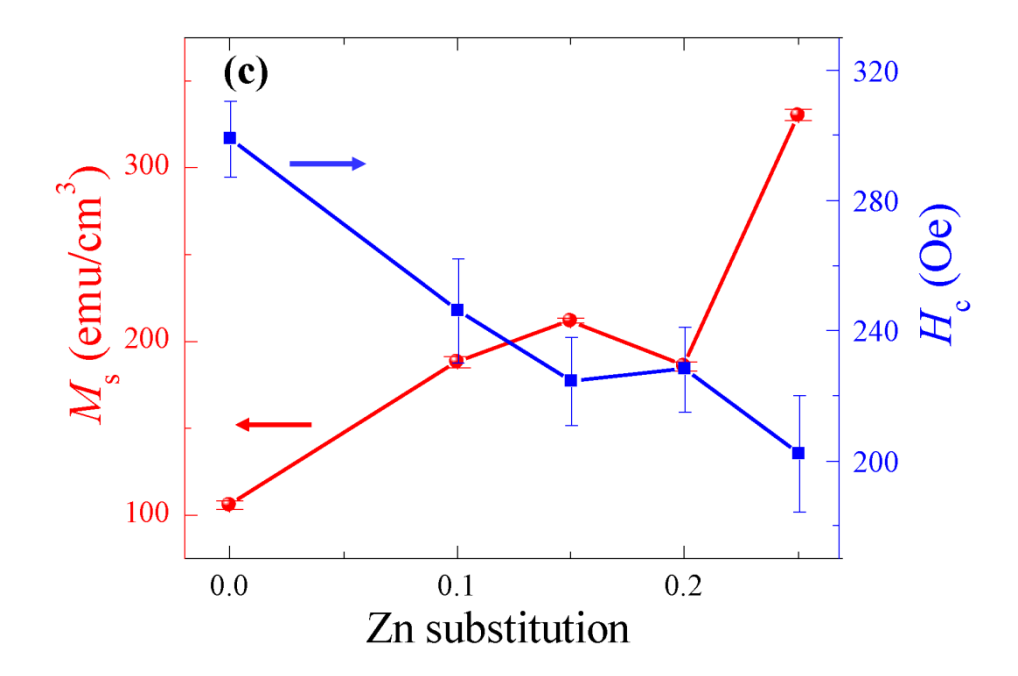


Figure 3

